ACADEMIC PRESS

Available online at www.sciencedirect.com

SCIENCE DIRECT®

Journal of Sound and Vibration 270 (2004) 341–359

JOURNAL OF SOUND AND VIBRATION

www.elsevier.com/locate/jsvi

Estimating the ratio between travelling and standing vibration waves under non-stationary conditions

Izhak Bucher

Faculty of Mechanical Engineering, Technion - Israel Institute of Technology, Haifa 32000, Israel

Received 6 December 2001; accepted 5 December 2002

Abstract

This paper presents a new method of spatially decomposing vibration patterns in real time into their travelling and standing parts. This method creates a localized parametric model describing the nature of the developed vibrations leading to a scalar measure of the travelling to standing waves ratio. Despite being rather simple compared with spatial Fourier transform that yields space-averaged results, the current method seems superior for a localized description. Due to its superior localization, the decomposition conveys important insight and valuable information for vibrating structures that can be used for identification, diagnosis and for control purposes of ultrasonic motors and rotating discs. Several features make the proposed method advantageous over existing schemes, in particular when the number of deployed sensors is small and confined to a small region. It is shown that the presented approach differs from the commonly used Fourier-based methods in several ways: (a) the proposed method does not require equally distributed sensors and does not require a spatially complete coverage of the analyzed domain nor does it require equally spaced sensing elements; (b) the algorithm makes neither use of the spatial wavelength nor requires its estimate to curve-fit the instantaneous spatial deformation patterns; (c) the method is most suitable for cases where a localized pattern needs to be estimated and is therefore robust to imperfections in the vibrating structure; (d) the presented formulation has a recursive form that is suitable for real-time implementations by a digital signal processor.

1. Background and introduction

Travelling and standing waves need to be separated when dealing with translating or rotating media and when such vibration patterns are to be created in a structure [1,2]. This separation is also required when trying to separate travelling deformation patterns in a rotating structure [3]. The deformation and stress waves progressing in a vibrating structure can often be decomposed

E-mail address: bucher@technion.ac.il (I. Bucher).

0022-460X/03/$ - see front matter
doi:10.1016/S0022-460X(03)00539-X

according to their wavelengths, frequency and direction of progression. The separation of measured deformations into their wavelength components requires simultaneous spatial information, typically obtained from an array of sensors or from a continuously scanning sensor [3,4]. The measured signals are commonly transformed to obtain the wavelength/wave-number domain using a Fourier transformation [3] and thus the employed method has to comply with some constraints and be prone to errors that are associated with this transformation. This paper develops an approach that does not make use of Fourier transformations and thus some of the limitations that are often associated with these methods are removed. The proposed method can serve as the basis for a real-time estimation method of the sought temporal and spatial properties while not being limited by the spatial (Nyquist) sampling criterion nor does it require equal spacing between sensing elements. Although lightly damped structures are characterized by their eigenvectors being standing waves in space, the combination of several modes, can give rise to travelling waves [4–9]. Travelling waves occur most naturally in cases where there are close natural frequencies as in rotationally periodic structures, and when an external excitation of motion encourages such response patterns [5–7]. Travelling waves are also being used in ultrasonic motors where two mode shapes with a nearly identical natural frequency [1] are driven to create a travelling pattern. The two close modes can potentially form a mixture of travelling and standing waves (see [5, pp. 225–229; 10]), while a pure travelling motion develops when the correct spatial and temporal driving signals are being used. In ultrasonic motors, pure travelling waves is desired but as the device are predominantly treated in an ''open-loop'' manner thus effectively ignoring the effect of external loading [2], local imperfections cause deterioration of the performance [8]. A tool such as the presented one can greatly improve the performance by allowing one to tune the applied excitation signals to provide an optimal ratio of travelling to standing waves.

Rotating machines have axisymmetric components that may develop travelling response patterns (with respect to inertial or body co-ordinates) as a clear indication of a particular structural defect or due to specific external loading or excitation [5–7]. Rotating machines are known to whirl in co- and counter-rotating directions while rotating discs deform in a shape that is a combination of several different wavelengths that may also travel or stand in space. The detection and separation of such patterns in real time requires an array of sensors [3,6,7] to allow for a spatial Fourier transform followed by a time–frequency transformation (or creation of a speed–frequency map, often addressed as Zmod by the aeroengine industry). The four-fold separation in Ref. [3] is applied to decompose the structural response into its frequency, amplitude, wavelength and direction of travel of the vibration pattern. A different approach is shown in Ref. [11] where continuous scanning provides the spatial information, but this method is impractical for real devices and can be only used in the laboratory.

The deployment of a suitable array of sensors is often impossible. Thus a method that is based on measurements taken on a sector or a few sectors of a rotating disc is desirable. A localized deployment of sensors has the advantage that it provides the local properties of the vibrating structure and is less sensitive to slower vibrations having long wavelengths. This is contrary to the averaging action of the Fourier transformation whose input is obtained by measuring on the entire circumference of say a rotating bladed-fan in a jet engine. The proposed method can provide a real-time diagnostics means or serve in a closed-loop control system attempting to generate travelling waves for propulsion purposes or in applications where spatially uniform amplitude is desired [1] for the reduction of sliding friction [2].

The paper is structured as following: in Section 2 the proposed method is outlined and the mathematical properties of mixed standing and travelling waves are outlined: curve-fitting procedures both in time and space are developed and explained; in Section 3 numerical and experimental results of the proposed algorithm are shown and analyzed; Section 4 concludes the paper with a summary.

2. Decomposition and signal processing of vibration waves

In this section it is shown how a vibration pattern can be decomposed into its travelling components. A typical laboratory set-up is depicted in Fig. 1 where an array of sensors is deployed circumferentially to simultaneously measure the vibration signals from all the sensors. In this figure, a single wavelength is seen to prevail (on the right) and an electromagnetic excitation device is used to stimulate the vibration patterns in the rotating structure. The main result of this paper will show that for a dominant vibration pattern spatially characterized as a sinusoid, an ellipse will be created from the measured data in the complex domain. This ellipse represents the sought travelling wave properties and will be used to extract these features in a numerically efficient manner. Both an analytical, non-parametric approach via the Hilbert transform and a smoother parametric adaptation method, are presented as a means to extract the instantaneous amplitude and phase along the space co-ordinate.

2.1. Mathematical decomposition of spatio-temporal information into standing and travelling waves

Consider a vibration wave progressing in a structure along a single direction in space, (namely the x direction, but in Figs. 1 and 2 this will be the angular direction θ). Such a vibrating pattern having a single temporal frequency, ω, and a single wavelength in space, $\lambda = \frac{2\pi}{\kappa}$, can be described

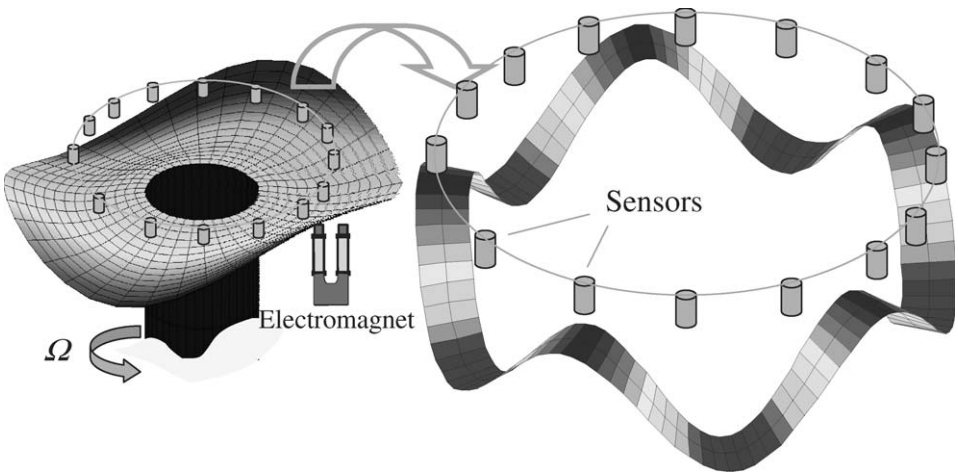

Fig. 1. Left: A deformed rotating disc excited by an electromagnetic device. Right: A strip (segment) "visible" by the array of sensors, shown is a uniform wavelength and a uniformly spaced sensor array.

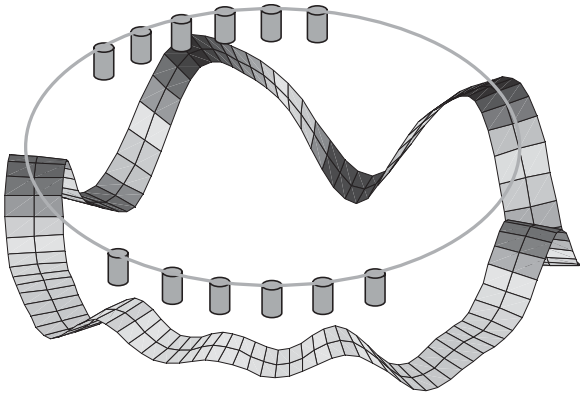

Fig. 2. A segment of a vibrating disc having a non-uniform wavelength and a non-uniformly spaced sensor array.

mathematically as

$$w(x,t) = A(\kappa x)\cos\omega t + B(\kappa x)\sin\omega t + R(\beta x, \varepsilon t), \tag{1}$$

where $A(\kappa x)$, $B(\kappa x)$ are position-dependent amplitude functions and κ is the wave number, $R(\beta x, \varepsilon t)$ is a residual function having typically a long wavelength characterized by β and a low-frequency $\varepsilon \ll \omega$.

Often, an external source that serves as a phase reference is present. For example in rotating machines the phase is referenced to the rotational position of the shaft. Another example for an external phase reference is the sinusoidal excitation signal driving ultrasonic motors.

In order to retrieve the standing and travelling parts of the measured response, one has to compute $A(\kappa x)$, $B(\kappa x)$ with the appropriate phase correction. Let the amplitudes be functions of a single wavelength, and therefore harmonic functions of space, e.g.,

$$A(\kappa x) = A_1\cos\kappa x + A_2\sin\kappa x; \quad B(\kappa x) = B_1\cos\kappa x + B_2\sin\kappa x. \tag{2}$$

By using trigonometric identities, Eqs. (1) and (2) can be recast in the form

$$\begin{aligned} w(x,t) = \tfrac{1}{2}((A_1 + B_2)\cos(\omega t - \kappa x) + (B_1 - A_2)\sin(\omega t - \kappa x) + \cdots \\ (A_1 - B_2)\cos(\omega t + \kappa x) + (B_1 + A_2)\sin(\omega t + \kappa x)). \end{aligned} \tag{3}$$

Eq. (3) separates the parts travelling in the positive and negative directions (having the arguments $(\omega t - \kappa x)$, $(\omega t + \kappa x)$ respectively).

A similar decomposition can be achieved by defining

$$\hat{W}(\kappa x) = A(\kappa x) + \mathrm{i}B(\kappa x). \tag{4}$$

The complex amplitude approach separates the in-phase (real) and in-quadrature (imaginary) components and paves the way to the Hilbert-transform-based decomposition.

Substituting Eq. (2) in Eq. (4), one has

$$\begin{aligned} 2\hat{W}(\kappa x) = A_1(\mathrm{e}^{\mathrm{i}\kappa x} + \mathrm{e}^{-\mathrm{i}\kappa x}) - \mathrm{i}A_2(\mathrm{e}^{\mathrm{i}\kappa x} - \mathrm{e}^{-\mathrm{i}\kappa x}) \\ + \mathrm{i}B_1(\mathrm{e}^{\mathrm{i}\kappa x} + \mathrm{i}\mathrm{e}^{-\mathrm{i}\kappa x}) + B_2(\mathrm{e}^{\mathrm{i}\kappa x} - \mathrm{i}\mathrm{e}^{-\mathrm{i}\kappa x}) \end{aligned} \tag{5}$$

or rearranging

$$\hat{W}(\kappa x) = W_+ e^{i\kappa x} + W_- e^{-i\kappa x}, \tag{6}$$

where

$$W_+ = \tfrac{1}{2}[(A_1 + B_2) + i(B_1 - A_2)], \quad W_- = \tfrac{1}{2}[(A_1 - B_2) + i(B_1 + A_2)]. \tag{7}$$

Here W_+ represents the amplitude (and phase, being complex) of the wave travelling in a positive $(+x)$ direction while W_- represents the part progressing in the negative direction $(-x)$.

By inspecting the coefficients of Eqs. (7) and (3) it can be deduced that they carry the same information.

Indeed Eq. (6) as plotted in Fig. 3, shows that the curve traced by $\hat{W}(\kappa x)$ in the complex plane is an ellipse whose properties represent the sought nature of the vibrating pattern. When a pure travelling wave exists, say in the positive direction, only W_+ will be non-zero as evident from Fig. 3, the ellipse will become a pure circle.

The spatial distribution of the in-phase $(\cos \omega t)$ and in-quadrature $(\sin \omega t)$ components determines the ratio between the standing and travelling part and the direction of travel in space. A scalar measure that determines how far one is from having pure travelling or standing waves is adopted from Antenna design and is called the standing waves ration (SWR). One defines this number as

$$SWR = (|W_+| + |W_-|)/(|W_+| - |W_-|) \tag{8}$$

and it can be seen that it becomes unity $(+/-)$ for pure travelling waves and tends to infinity for standing waves when $|W_+| = |W_-|$.

Often the wavelength of the vibrating pattern is not known with sufficient accuracy and the fast and accurate estimation of $A(\kappa x), B(\kappa x)$ must rely on a two-stage approach as described below. In the first part the $A(\kappa x), B(\kappa x)$ coefficients are curve-fitted by two alternative time-domain methods and in the second stage the local spatial properties are found by curve-fitting an ellipse to the instantaneous spatial distribution of deformations.

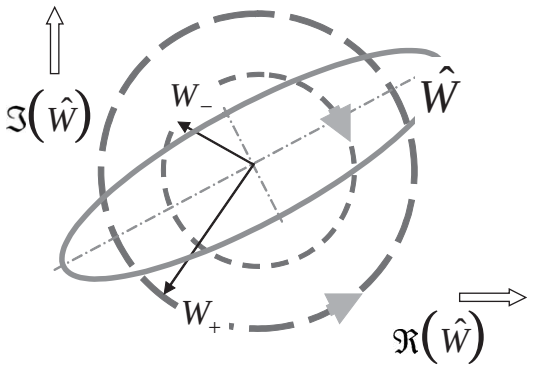

Fig. 3. An ellipse representing a mixture of standing and travelling waves composed of two waves moving in opposite directions.

2.1.1. Fitting the instantaneous amplitude and phase

The time signal measured from an array of sensors need to be processed in order to obtain the instantaneous in-phase and in-quadrature (or alternatively the amplitude and phase) components. Two approaches are presented: The first approach makes use of the Hilbert transform to show analytically that a space-dependent analytic signal [10,12] of a travelling wave, allows us to obtain the in-phase and in-quadrature components as a function of the space co-ordinate, x. The second approach is more suitable for cases where the excitation frequency, ω, is known and therefore a recursive least-squares approach is employed with smoother and more robust performance than the (more general) Hilbert-transform-based method.

2.1.2. The Hilbert-transform-based approach

In order to obtain the relative phase information as a function of space, the distributed response is converted into an analytic signal form [12]. By application of the Hilbert transform to Eq. (1), one obtains

$$\mathrm{H}[w(x,t)] = -A(\kappa x)\cos\omega t + B(\kappa x)\sin\omega t + \mathrm{H}[R(\beta x, \varepsilon t)], \tag{9}$$

where $\mathrm{H}[\cdot]$ represents the Hilbert transform operating in the time domain. $R(\beta x, \varepsilon t)$ is assumed to possess a long wavelength in space and is thus considered as a constant for a space-localized approximation.

The analytic response (signal) is defined as

$$\tilde{w}(x,t) = w(x,t) + \mathrm{i}\mathrm{H}[w(x,t)] \tag{10}$$

and when applied to Eqs. (1) and (2) one obtains (combining Eq. (1) + i∗ Eq. (9)),

$$\tilde{w}(x,t) = ((1-\mathrm{i})A(\kappa x) + (1+\mathrm{i})B(\kappa x))\mathrm{e}^{\mathrm{i}\omega t} + \tilde{R}, \tag{11}$$

where $\tilde{R} = R + \mathrm{i}\mathrm{H}[R]$, or simplifying

$$\tilde{w}(x,t) = (1-\mathrm{i})\{(A(\kappa x) + \mathrm{i}B(\kappa x))\mathrm{e}^{\mathrm{i}\omega t} + \tilde{R}/(\mathrm{i}-1)\}. \tag{12}$$

Dividing Eq. (11) by $(1-\mathrm{i})\mathrm{e}^{\mathrm{i}\omega t}$ (which is in effect a de-modulation process) and ignoring the residual term temporarily, one transforms the obtained expression into the wave-attached co-ordinate system.

Once Eq. (2) is substituted into Eq. (12) one obtains the same expressions as obtained in Eqs. (6) and (7) and thus the Hilbert transform can be used to extract the required information about the instantaneous amplitudes of the positive and negative direction.

The actual Hilbert transform for the proposed application, makes use of a finite impulse response (FIR) time-domain filtering approach (see Ref. [12]) to create an analytical signal from all the involved sensors. Rather than obtaining a continuous function of x, a space-sampled version is obtained in this method, but it is important to note that the Hilbert transform provides an instantaneous estimate for each and every sensor and thus a space-sampled version of the complex amplitude is created to which an ellipse can be curve-fitted.

2.1.3. The recursive least-squares approach for amplitude-fitting

An alternative approach to the time-domain Hilbert transform uses a parametric model with the assumption that the temporal frequency, ω, is known. The adaptive least-squares approach

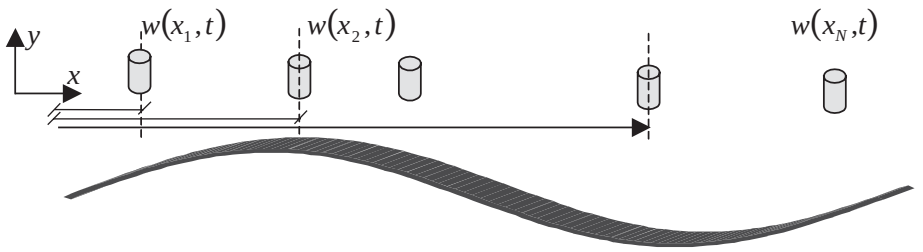

Fig. 4. Sensor array measuring the vibration in the y direction.

uses p_{max} time samples taken at the nth location x_n (see Fig. 4) with each sample obeying

$$w(x_n, t_p) = A(\kappa x_n)\cos\omega t_p + B(\kappa x_n)\sin\omega t_p + C,$$
$$n = 1, \ldots, N, \quad p = 1, \ldots, p_{max}. \tag{13}$$

For each measured location one is able to extract the scalars $A(\kappa x_n), B(\kappa x_n)$, by collecting p_{max} such equations (for each of the N sensors) to obtain

$$\begin{pmatrix} w(x_n,0) \\ w(x_n,t_1) \\ \vdots \\ w(x_n,t_{p_{max}}) \end{pmatrix} = \begin{bmatrix} 0 & 1 & 1 \\ \cos\omega t & \sin\omega t_1 & 1 \\ \vdots & \vdots & \vdots \\ \cos\omega t_{p_{max}} & \sin\omega t_{p_{max}} & 1 \end{bmatrix} \begin{pmatrix} A(\kappa x_n) \\ B(\kappa x_n) \\ C_n \end{pmatrix}. \tag{14}$$

Eq. (14) is not suitable for an on-line implementation and is thus not capable of tracking the variation of the vibrating pattern. A recursive estimator in therefore suggested for each sensed location [10] as

$$\theta_{q+1,n} = \theta_{q,n} + L_{q,n}(w_{q,n} - \hat{w}_{q,n}), \tag{15}$$

where $\hat{w}_{q,n} = \psi_q^{\mathrm{T}}\theta_{q,n}$ is the predicted response at the nth sensor, and $w_{q,n}$ is the measured response. The unknown vector of parameters at time instant $t_q = q\Delta t$ is $\theta_{q,n} = \{A_q(\kappa x_n)\ B_q(\kappa x_n)\ C_{q,n}\}$. One also defines $\psi_q = (\cos\omega t_q\ \sin\omega t_q\ 1)$ that can be pre-computed since ω is known.

The gain vector $L_{q,n}$ is computed so as to minimize the error function $\sum_{k=1}^{q}\lambda^{q-k}(w_{k,n} - \hat{w}_{k,n})^2$ [13]. The selection of the forgetting factor λ weights the old data against the newly acquired information and controls the tracking capability of the algorithm. It can be shown [10,13] that the adaptive gain matrix for the nth location obeys Ref. [13], giving

$$L_{q,n} = P_{q-1}\psi_q/(\lambda + \psi_q^{\mathrm{T}}P_{q-1}\psi_q), \tag{16}$$

where by updating in parallel to Eq. (15)

$$P_q = \frac{1}{\lambda}\left(P_{q-1} - \frac{P_{q-1}\psi_q\psi_q^{\mathrm{T}}P_{q-1}}{\lambda + \psi_q^{\mathrm{T}}P_{q-1}\psi_q}\right). \tag{17}$$

P_q has to be initialized as $P_q = \eta^2 I$ where η is close to unity. In order to maintain the tracking ability of the algorithm, P_q needs often to be reset to its initial value [10].

Having measured the response one is able to track both the amplitude and phase with the above-mentioned algorithm as illustrated in a block diagram form in Fig. 5 and is demonstrated in Fig. 6.

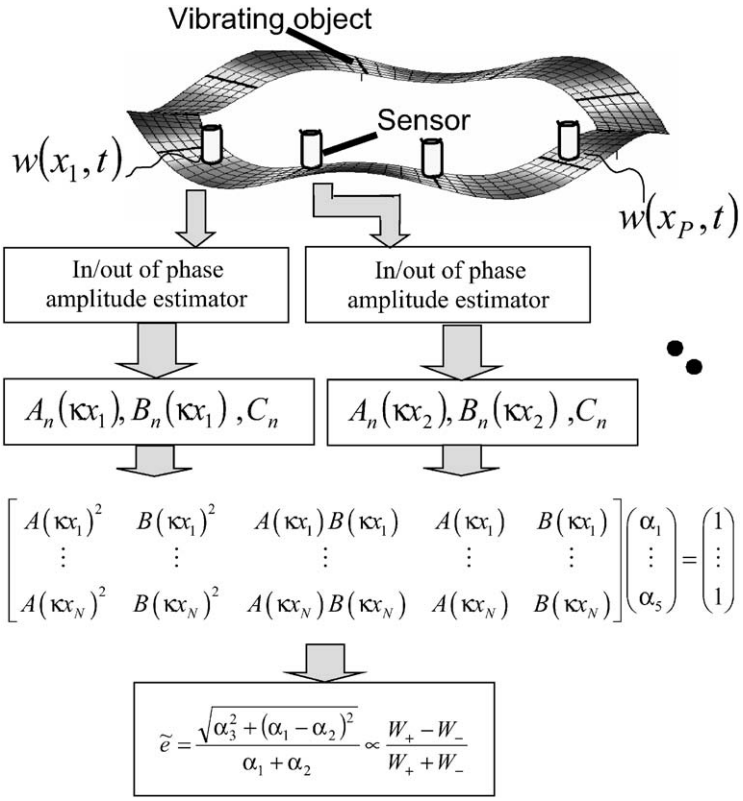

Fig. 5. Flowchart of the real-time travelling wave estimation algorithm.

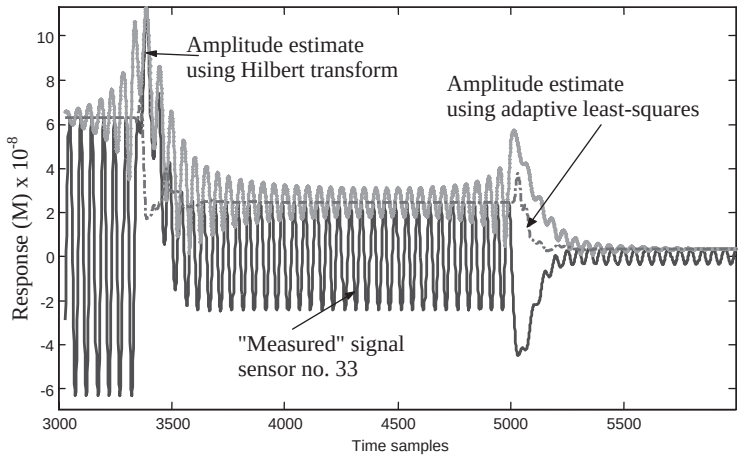

Fig. 6. Time signal from a simulated measurement showing a single sensor and its estimated envelope using Hilbert transform and using Eqs. (15)–(17) and $\lambda = 0.9$.

2.2. Estimation of the travelling and standing components from an array of sensors

Consider an array of sensors deployed along the direction of travel of a deformed state as shown in Fig. 2.

In order to determine whether a wave is propagating or standing in space, sensors should be placed at two spatial locations (in the case of rotating machinery) or more. Indeed, in rotating machinery, two sensors that are spaced a 1/4 of wavelength apart are being used to distinguish co- and counter-rotating whirl patterns of bending shafts, as shown in Ref. [3]. Unfortunately two sensors may prove insufficient in terms of spatial resolution and the resulting estimate may be misleading in presence of measurement noise or when the motion is composed of several wavelengths. In reality, the deformation pattern may be a combination of several wavelengths which gives rise to a deformation that is no longer described by a single sinusoid. For this reason more than two sensors are often employed on rotating discs to allow for separation of different wavelengths. A different approach makes use of a scanning, non-contacting sensor (e.g., Refs. [4,11]) that can provide a spatially dense grid of measurements satisfying the spatial resolution requirements. The continuous approach is not suitable for real-time applications since different points in space are measured at different times with this method. The continuous scanning approach (see Ref. [4]) uses a single scanning sensor that must have a clear optical path to the structure and is thus often impractical.

As the wavelength is usually unknown while the temporal frequency is dictated by the external forcing mechanism and is thus known, it proves convenient to eliminate κ and t from the formulation by a two-step approach. In the first part that was described above, the time dependence is eliminated while the second stage eliminates the spatial frequency (wave vector) κ.

2.2.1. Fitting an ellipse to the complex amplitude

It can be shown (e.g., Ref. [3]), that for a single wavelength, a plot of $A(\kappa x_n)$ versus $B(\kappa x_n)$ would generally yield an ellipse. In the case of standing waves, the ellipse will degenerate into a straight line while pure travelling waves produce a perfect circle. Having measurements at several locations along x, one is able to use the above-mentioned procedure to compute several pairs of co-ordinates $A(\kappa x_n)$, $B(\kappa x_n)$, these measured pairs should reside on an ellipse. In order to curve-fit the properties of the obtained ellipse, a parametric description of a general non-canonical ellipse is being used, namely

$$b(B(\kappa x_n) - B_0)^2 + a(A(\kappa x_n) - A_0)^2 + cA(\kappa x_n)B(\kappa x_n) = 1, \tag{18}$$

where A_0, B_0 determine the centre of the ellipse and a, b, c are the parameters to be determined.

For sake of mathematical convenience, Eq. (18) can be transformed into a bi-linear form as

$$\begin{pmatrix} A(\kappa x) - A_0 \\ B(\kappa x) - B_0 \end{pmatrix}^{\mathrm{T}} \begin{bmatrix} d_{11} & d_{12} \\ d_{21} & d_{22} \end{bmatrix} \begin{pmatrix} A(\kappa x) - A_0 \\ B(\kappa x) - B_0 \end{pmatrix} = \rho^2, \tag{19}$$

where a scaling parameter ρ is used. This parameter scales the overall size of the ellipse but does not change the proportions of the standing and travelling waves. It can be shown, by expanding Eq. (19) (with an appropriate selection of ρ^2) that the measurements, $(A(\kappa x_n), B(\kappa x_n))$, $n = 1, \ldots, N$, can be used to form a linear set of equations, in some new (intermediate) parameters

α_i, $i = 1, \ldots, 5$. The coefficient matrix in this equation contains powers of the now known co-ordinate pairs (amplitudes), $A(\kappa x_n), B(\kappa x_n)$.

Since $d_{12} = d_{21}$, five unknowns remain, $d_{11}, d_{12}, d_{22}, A_0, B_0$. Defining

$$\alpha_1 = d_{11}, \quad \alpha_2 = d_{22}, \quad \alpha_3 = 2d_{12}, \quad \alpha_5 = -2d_{12}A_0 - 2d_{22}B_0,$$
$$\rho^2 = \begin{pmatrix} A_0 \\ B_0 \end{pmatrix}^{\mathrm{T}} \begin{bmatrix} d_{11} & d_{12} \\ d_{12} & d_{22} \end{bmatrix} \begin{pmatrix} A_0 \\ B_0 \end{pmatrix}, \tag{20}$$

one can rewrite Eq. (19) as

$$\begin{bmatrix} A(\kappa x_1)^2 & B(\kappa x_1)^2 & A(\kappa x_1)B(\kappa x_1) & A(\kappa x_1) & B(\kappa x_1) \\ \vdots & \vdots & \vdots & \vdots & \vdots \\ A(\kappa x_N)^2 & B(\kappa x_N)^2 & A(\kappa x_N)B(\kappa x_N) & A(\kappa x_N) & B(\kappa x_N) \end{bmatrix} \begin{pmatrix} \alpha_1 \\ \vdots \\ \alpha_5 \end{pmatrix} = \rho^2 \begin{pmatrix} 1 \\ \vdots \\ 1 \end{pmatrix}. \tag{21}$$

Dividing Eq. (21) by ρ^2, one shrinks the ellipse in size without affecting its proportions and one can solve for $\alpha_1, \ldots, \alpha_5$ in the least-squares sense [14]. From Eq. (20) one can now compute the co-ordinates of the centre of the ellipse (A_0, B_0) as

$$A_0 = (\alpha_3\alpha_5 - 2\alpha_2\alpha_4)/(4\alpha_1\alpha_2 - \alpha_3^2), \quad B_0 = (\alpha_3\alpha_4 - 2\alpha_1\alpha_5)/(4\alpha_1\alpha_2 - \alpha_3^2). \tag{22}$$

The semi-minor/major (see Fig. 3), can be used to decompose a typical ellipse into its positive and negative travelling components. It can be shown that [15]

$$|W_+| = \tfrac{1}{2}((1/\sqrt{\lambda_{max}}) + (1/\sqrt{\lambda_{min}})), \quad |W_-| = \tfrac{1}{2}((1/\sqrt{\lambda_{min}}) - (1/\sqrt{\lambda_{max}})), \tag{23}$$

where λ_{min}, λ_{max} are the eigenvalues of the weighting matrix in Eq. (19), i.e., the solution of

$$\lambda\phi = \begin{bmatrix} 2\alpha_1 & \alpha_3 \\ \alpha_3 & 2\alpha_2 \end{bmatrix} \phi. \tag{24}$$

The eccentricity of the ellipse is commonly defined by the dividing the length of the semi-major by the length of the semi-minor,

$$e = (|W_+| - |W_-|)/(|W_+| + |W_-|). \tag{25}$$

The last term is the reciprocal of the commonly used SWR, which was previously defined. It is clear that e is bounded between $-1 \leqslant e \leqslant 1$ with $e = -1$ indicating pure travelling waves in the negative x direction, $e = \pm 1$ indicates a pure travel towards the positive or negative direction and $e = 0$ for completely standing waves. Eq. (23) can be substituted in Eq. (25) to yield,

$$e = ((1/\sqrt{\lambda_1}) - (1/\sqrt{\lambda_2}))/((1/\sqrt{\lambda_1}) + (1/\sqrt{\lambda_2})) = (\sqrt{\lambda_2} - \sqrt{\lambda_1})/(\sqrt{\lambda_2} + \sqrt{\lambda_1}). \tag{26}$$

For the purpose of replicating the three cases of pure negative of positive travelling waves or pure standing wave, the function (assuming $\alpha_1 \neq -\alpha_2$)

$$\tilde{e} = (\lambda_2 - \lambda_1)/(\lambda_2 + \lambda_1) = \sqrt{\alpha_3^2 + (\alpha_1 - \alpha_2)^2}/(\alpha_1 + \alpha_2) \tag{27}$$

serves a similar purpose, especially in cases where the travelling waves part is to be maximized using a real-time control implementation or for monitoring applications. This form does not require the solution of Eq. (24) and is thus faster to compute.

Indeed Eqs. (21) and (27) can be realized in real-time since only five parameters need solving Eq. (21) can be solved in the least-squares sense by a direct approach or by updating the QR decomposition [14] of Eq. (21) that is constructed with the newly estimated $A(\kappa x_n), B(\kappa x_n)$.

Fig. 5 summarizes the required set-up and the parts of the algorithm leading to the separation of the travelling from the standing waves. In this figure, the flow of data from the measured sensors via the parallel implementation of the time-domain adaptive curve-fit to the fit of the ellipse yielding the sought ratio is visualized.

3. Numerical and experimental investigation of the algorithm

In order to test the mentioned algorithm, a finite element model of an axisymmetric structure was built. The model was constructed to represent a test rig that was utilized in the laboratory and which is depicted in Fig. 7. Several key components are identified, these being an axisymmetric ring structure and the three piezoelectric forcing devices.

The model was used to create spatially discretized equations of motion of the form

$$M\ddot{q} + D\dot{q} + Kq = F_c \cos \omega t + F_s \sin \omega t. \tag{28}$$

The external forces, F_c, F_s represent three excitation devices (See Fig. 7) that were phased in time to create the appropriate proportions of the standing and travelling waves. The proportions of the model were designed to possess several natural frequencies in the useful bandwidth of the piezoelectric actuators (20 kHz). Two of the mode shapes that appear later in the experiments are depicted in Fig. 8. Each of the presented mode shapes has a twin mode shape (eigenvector) having a close natural frequency (that would have been identical under perfectly symmetric boundary conditions).

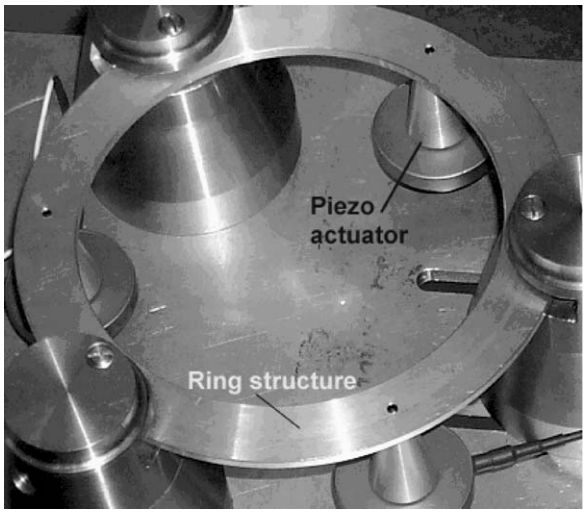

Fig. 7. Laboratory test rig after which the finite element model was built.

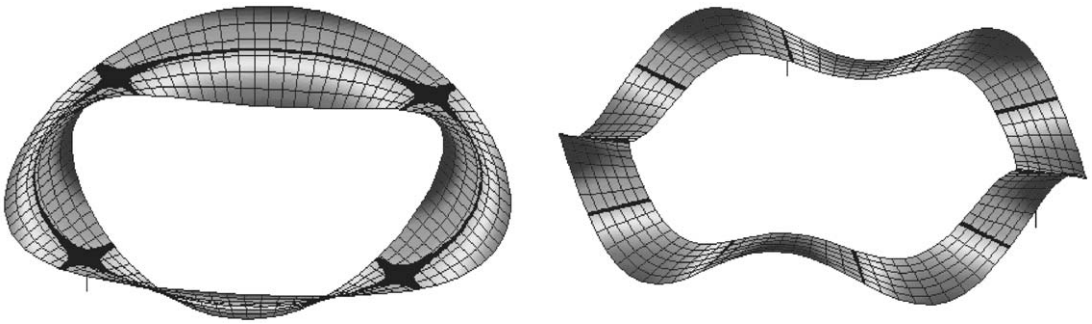

Fig. 8. Finite element model showing two mode shapes that were excited in the experiment.

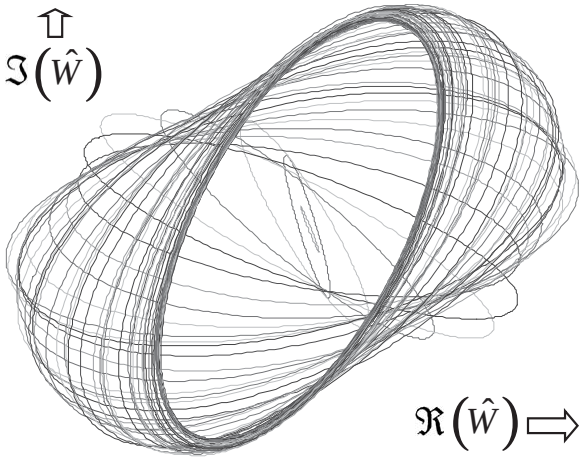

Fig. 9. Evolution of the fitted ellipse versus time as estimated by the algorithm. Only one force transition is shown here for clarity.

3.1. Travelling wave estimation algorithm—a numerical example

The finite element model consisting of 1500 degrees of freedom was simulated where the input vector consisted of a vector of harmonic forces. The amplitude and phase of this excitation vector were changed during the simulation in order to assess the tracking capabilities of the algorithm that is diagrammatically illustrated in Fig. 5.

3.1.1. Performance of the amplitude and phase fitting method

The fitted ellipse, the eccentricity ratio, (which is a direct indication for the standing/travelling waves ratio) and the instantaneous centre of the ellipse are all indicative of the vibration state. The ability of the algorithm to track the change in these parameters is illustrated via a comparative estimate of the instantaneous enveloped computed by $|\tilde{W}(x)|$ or $\sqrt{A^2(\kappa x) + B^2(\kappa x)}$. Fig. 6 shows the tracking capability of the in- and out-of-phase components by comparison with the measured signal. Fig. 6 illustrates quite clearly how the proposed algorithm is capable of tracking the standing/travelling wave ratio during a transient while Fig. 9 shows the time evolution of the fitted

ellipse during a transient. It is worth mentioning that the Hilbert-based envelope oscillates due to the presence of slow vibrations causing an offset in the analyzed time frame.

In this example the ring was at rest when the excitation was activated. The building of the ellipse is evident from Fig. 9 (shown every few samples for clarity), it can be seen that initially the amplitude of vibration is small and so is the fitted ellipse that grows with the build-up of vibration levels. Fig. 10 shows the estimate eccentricity and the tracking capability of the algorithm during transients. The eccentricity, as was mentioned before is a direct measure of the ratio between the travelling and the standing vibration waves, while the extent of the ellipse reflects the amplitude.

As the algorithm can use a small number of sensors that occupy a part of a wavelength, the algorithm was used in the simulated examples to fit an ellipse based on six sensors. The actual algorithm fits, at any given instant of time, an ellipse and finds the centre of this ellipse as shown in (left side of) Fig. 11. Since the vibrating pattern is not made of a single wavelength, the residual

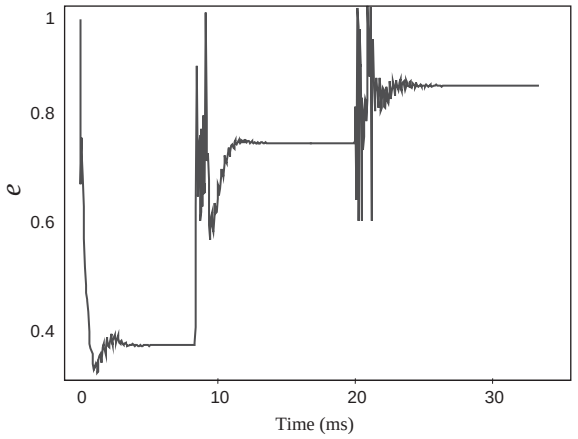

Fig. 10. Eccentricity ratio versus time as estimated by the algorithm (Eq. (24)). Note that the transients are genuine due to the sudden change in the external forces.

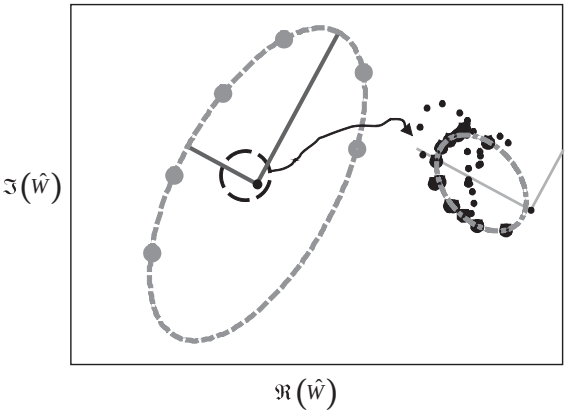

Fig. 11. Measured amplitudes and the fitted ellipse—simulation. On the right a closer view of the ellipse centre as it evolves in the recent history with a second ellipse fitted to it.

$R(\beta x, \varepsilon t)$ moves with time and indeed the right part of Fig. 11 shows that it traces a smaller ellipse that can be fitted with the same algorithm to the history of the centre of the ellipse. This smaller ellipse represents the added low frequency (long wavelength) vibration, which is in fact the residual $R(\beta x, \varepsilon t)$.

3.1.2. Identifying locally travelling waves regions—a simulated example

In order to illustrate the advantage of the proposed algorithm in the estimation of local phenomena, a model of the structure in Figs. 7 and 8 was used in a simulation with slight asymmetry in the boundary conditions (as was observed in the laboratory test-rig). The excitation pattern that was chosen consisted of three sinusoidal forces with different amplitudes and phases. The excitation patterns were abruptly changed at discrete time instances to create a transient phenomenon of the travelling waves as was shown above. In the simulated study, simulated sensors were placed at an equal radius along the circumference of the ring (see Figs. 1 and 2). At rest, the spatial vibrating pattern is a three-dimensional thin ring (line) while under vibration, this ring deforms. Due to the asymmetry, the spatial pattern no longer consists of a single wavelength, and indeed plotting the complex amplitude as in Fig. 3, the observed curve in Fig. 12 is no longer an ellipse as it is composed of several ellipses each characterized by different parameters. The ability of the proposed algorithm to use a local measure is illustrated in Fig. 12 where the local fit of an ellipse to region II (see Fig. 12) is in good agreement with region II of Fig. 13 as it clearly

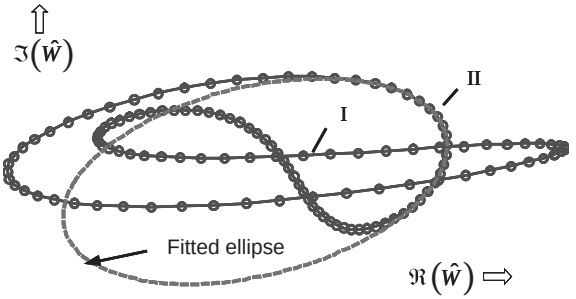

Fig. 12. A plot of $A(\kappa x_n)$ versus $B(\kappa x_n)$ showing a locally fitted ellipse—simulated structure.

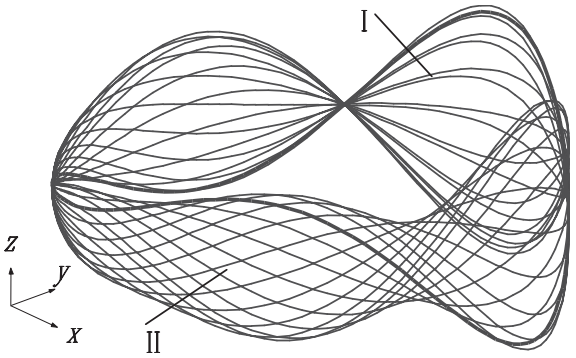

Fig. 13. Sequence of deformation states to mimic animation for visualizing travelling waves around the same time instant as in Fig. 12.

shows travelling waves. Moreover, the nearly straight line obtained in region I of Fig. 12 agrees with region I of Fig. 13 that shows clearly locally standing waves. Fig. 13 presents a succession of deformation states to mimic an animation of the deformation status as was simulated by Eq. (28).

3.2. Experimental study of the algorithm

In the experimental study, the system that is depicted in Fig. 5 was used. A laser vibration sensor measured the response at several points using the set-up that is shown in Fig. 14. A second experiment used five closely spaced sensors.

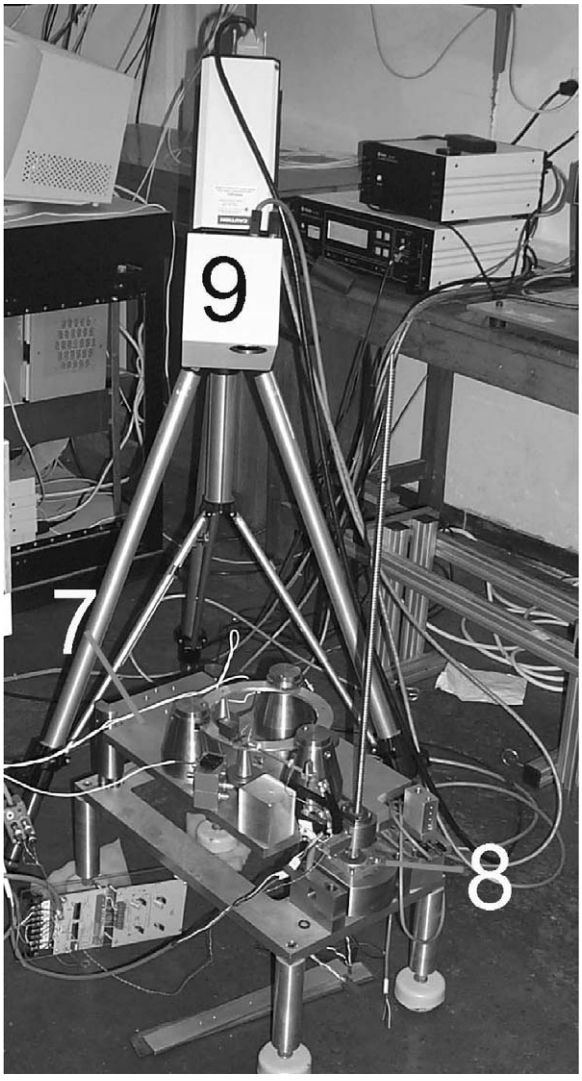

Fig. 14. The experimental system showing the vibrating ring and the measuring laser sensor.

Experiments were conducted under several excitation conditions giving rise to several combinations of standing/travelling waves. The measurements were performed on a segment of the ring and the results are plotted in Figs. 15–17.

Fig. 15 shows the response as a sequence of deformation states (mimicking an animation) using an excitation frequency yielding a mode shape that closely resembles the simulated mode shape one on the right side of Fig. 7. Changing the relative phase between the three excitation devices created a standing waves pattern (Fig. 15, top) to a nearly pure travelling waves (bottom) through an intermediate mixed standing/travelling stage (middle). The pure standing waves here are clearly defined with the appearance of a nodal point. Fig. 17 (which is measured on a part of the disc) shows the complex amplitude and the fitted ellipse as was described in the paper. The ellipse that was obtained shows that one has a mixture of travelling and standing waves while for the standing waves case, a straight line (not shown) was obtained. Fig. 16 shows three additional excitation patters at a difference frequency, this time giving rise to a differently shaped travelling and standing waves respectively. Once more the standing wave showed an in-phase motion of all the surface points with a clear indication of non-movable nodal points. It is worthy of mentioning that (as can be seen in Figs. 15 and 16), travelling waves create a nearly uniform distribution of amplitudes in space.

Often, a non-uniform behaviour along the circumference can be observed. Indeed, Figs. 18 and 19 illustrates clearly the importance of the proposed approach in such a case. In Fig. 18, a segment of the vibrating rings in which both travelling and standing patterns co-exist in different regions of

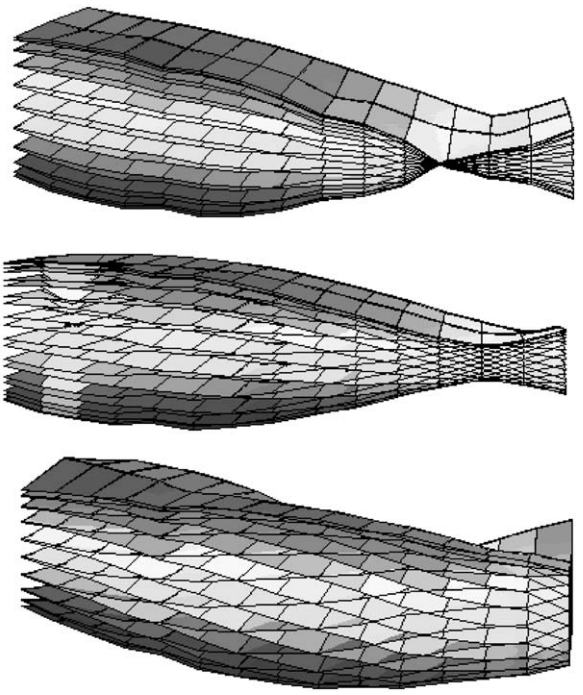

Fig. 15. Measured vibration response pattern on a section of the ring structure shown in Fig. 5. The three piezo-actuators have a relative temporal phase angle of 0°, 30° and 110° and the excitation frequency 2280 Hz.

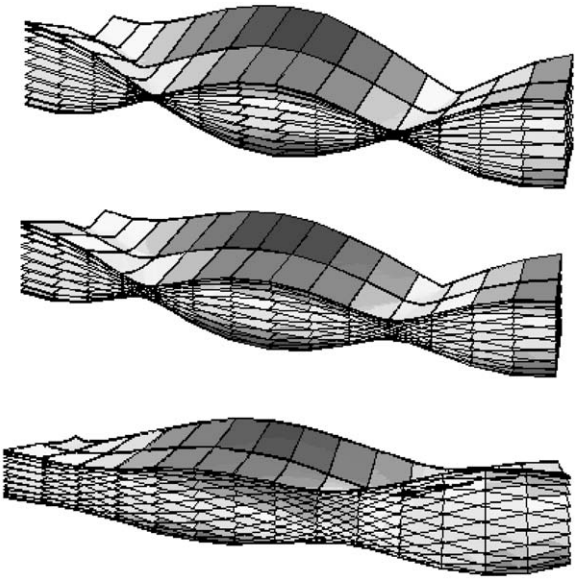

Fig. 16. Measured vibration response pattern under a relative temporal phase angle of 30°, 50° and 160° between the exciters. Excitation frequency 10518 Hz.

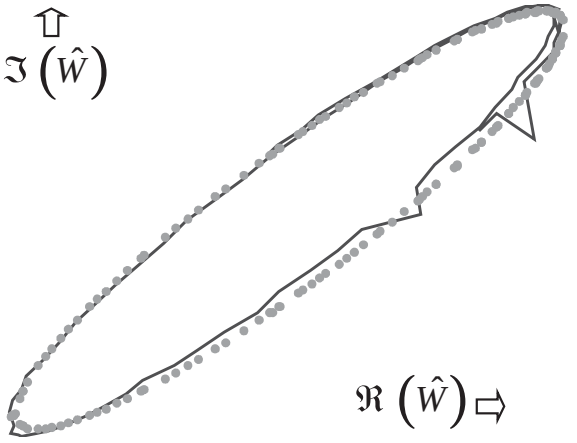

Fig. 17. Measured and fitted amplitudes of a mixed travelling and standing wave along a ring segment. Excitation frequency 2280 Hz.

the structure. Region A in Fig. 18 was measured using five sensors and it can clearly be seen that there is a significant amount of travelling waves present in this part. This conclusion can also be made by inspection of the left graph in Fig. 19. This plot makes use of the ellipse fit at a certain instant of time, also shown are the five sensors that are clearly sufficient to produce and estimate of the travelling waves ratio of $e = -0.49$. On the other hand region B in Fig. 18, clearly exhibits standing waves. The five sensors deployed over this region were sufficient to demonstrate in the right side plot of Fig. 19 that the fitted ellipse has degenerated into a straight line representing pure standing waves with an eccentricity $e \approx 0$, that was obtained. The importance of Figs. 18 and

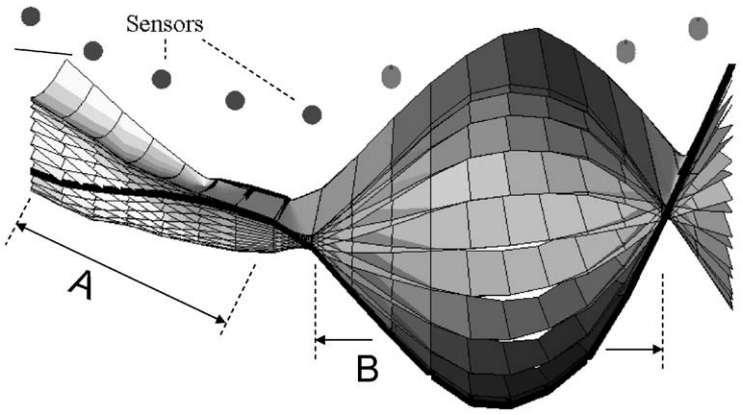

Fig. 18. Measured response (using a laser-scanning sensor) at several neighbouring time instances. Shown is a segment of the ring in Fig. 5 with two sets of sensors (regions A and B). Excitation frequency 3625 Hz.

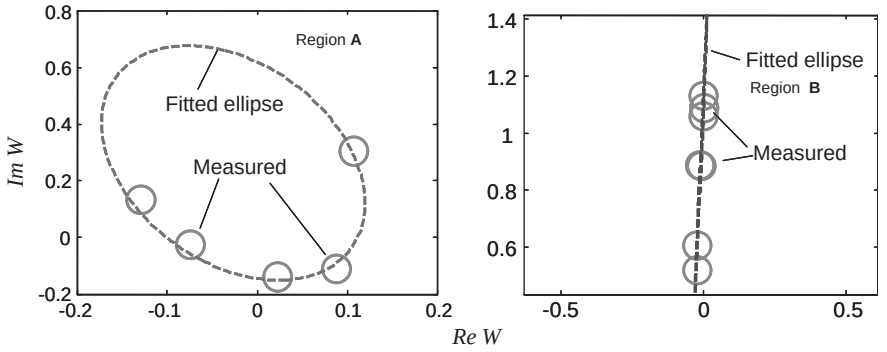

Fig. 19. Measured response and curve-fitted ellipse in two regions. Left: Region A in Fig. 18 showing travelling waves, $e = -0.49$. Right: Region B in Fig. 18 showing standing waves, $e = 0.01$.

19 is two-fold, first it shows why an averaging approach such as the spatial Fourier transform may be misleading and second it demonstrates how a small number of local sensors could be advantageous in this case.

4. Conclusions

A real-time signal processing method is presented that is aimed at the identification of standing and travelling waves using a relatively small number of sensors deployed along a part of a structure. The algorithm can be used in several applications, such as ultrasonic motors, and to decompose vibration patterns in rotating machinery. The algorithm works in real-time, making use of newly developed geometric and mathematical expressions that are directly related to the phenomenon of travelling waves. The algorithm was successfully demonstrated via simulation and experiments demonstrating its advantage in estimating localized deformation patterns.

Acknowledgements

This research was supported by the ISARELI academy for science (Grant No. 030072).

References

[1] S. Ueha, *Ultrasonic Motors: Theory and Applications*, Clarendon Press, Oxford, 1993.
[2] I. Bucher, O. Wertheim, Reducing friction forces by means of applied vibration, ASME – Design Engineering Technical Conferences, *18th Biennial Conference on Mechanical Vibration and Noise*, Pittsburgh, PA, September 9–12, 2001.
[3] I. Bucher, D.J. Ewins, Multi-dimensional decomposition of time-varying vibration response signals in rotating machinery, *Mechanical Systems and Signal Processing* 2 (4) (1997) 576–601.
[4] I. Bucher, Measuring spatial vibration using continuous laser scanning, *Third International Conference on Laser Measurement by Laser Techniques*, Ancona, Italy, June 1998, pp. 409–419.
[5] M. Geradin, D. Rixen, *Mechanical Vibrations: Theory and Application to Structural Dynamics*, Wiley, Chichester, 1994.
[6] P. Schmiechen, Travelling Wave Speed Coincidence, Ph.D. Thesis, Dynamics Section, Imperial-College, London, UK, 1997.
[7] G. Von Groll, Wind-milling in Aero-engines, Ph.D. Thesis, Dynamics Section, Imperial-College, London, UK, 2000.
[8] S.A. Tobias, R.N. Arnold, The influence of dynamical imperfection on the vibration of rotating disks, *Proceedings of the Institute of Mechanical Engineering* 171 (1957) 666–690.
[9] H. Nomura, T. Kamakura, K. Matsuda, Theoretical and experimental examination of near-field acoustic levitation, *Journal of the Acoustical Society of America* 111 (4) (2002) 1578–1583.
[10] S. Haykin, *Adaptive Filter Theory*, 3rd Edition, Prentice-Hall, Englewood Cliffs, NJ, 1996.
[11] I. Bucher, P. Schmiechen, D.A. Robb, D.J. Ewins, A laser-based measurement system for measuring the vibration on rotating discs, *First International Conference on Vibration Measurement by Laser Techniques*, Ancona, Italy, October, 1994.
[12] DSP Committee (Ed.), *Programs for Digital Signal Processing*, IEEE Press, Wiley, New York, 1979.
[13] L. Ljung, *System Identification*: *Theory for the User*, Prentice-Hall Information and System Sciences Series, Prentice-Hall, Upper Saddle River, 1999.
[14] A. Björck, *Numerical Methods for Least Squares Problems*, SIAM, Philadelphia, 1996.
[15] L. Meirovitch, *Computational Methods in Structural Dynamics*, Sijthoff & Noordhoff, Alphen a/d Rijn, 1980.